

000
001
002054
055
056

Texture Mapping 3D Models of Indoor Environments with Noisy Camera Poses

057
058
059003
004
005
006
007
008
009
010
011060
061
062
063

Anonymous 3DIMPVT submission

064
065

Paper ID 84

066
067

Abstract

068
069

Automated 3D modeling of building interiors is useful in applications such as virtual reality and environment mapping. Applying textures to these models is an important step in generating photorealistic visualizations of data collected by modeling systems. Camera pose recovery in such systems often suffers from inaccuracies, resulting in visible discontinuities when successive images are projected adjacently onto a plane for texturing. We propose two approaches to reduce discontinuities in texture mapping 3D models made of planar surfaces. The first one is tile based and can be used for images and planes at arbitrary angles relative to each other. The second one results in a more seamless texture, but is only applicable where camera axes for images are closely aligned with plane normals of the surfaces to be textured. The effectiveness of our approaches are demonstrated on two indoor datasets.

070
071

but can also result in larger localization error [16]. As a result, common methods for texture mapping generally produce poor results.

072
073

In this paper, we present a number of approaches to texture mapping 3D models of indoor environments made of planar surfaces in the presence of uncertainty and noise in camera poses. In particular, we consider data obtained from a human-operated backpack system with a number of laser range scanners as well as 2 cameras facing left and right, each equipped with fisheye lenses reaching an approximately 180° field of view and taking photos at a rate of 5 Hz. Applying multiple localization and loop-closure algorithms on the raw data collected by the onboard sensors [5, 14, 16], the backpack is localized¹ over its data collection period. This requires recovering the 6 degrees of freedom for the backpack as well as the cameras rigidly mounted on it. Once this is complete, the data from the laser range scanners is used to generate a 3D point cloud of the surrounding environment, from which a 3D planar model is created [20]. This model, consisting of 2D polygonal planes in 3D space, along with the set of images captured by the backpack’s cameras and their noisy 3D poses, can be considered the input to our texture mapping problem.

074
075

This problem straddles the fields of image-based localization refinement as well as image alignment and mosaicing, and thus our proposed solution shares many similarities with past research in those areas, which will be examined in Section 3. However, we can exploit known approximate camera poses as well as the 3D geometry of the environment to more accurately and efficiently texture the planes.

076
077

The remainder of the paper is organized as follows. Section 2 describes two variants of a tile-based mapping approach and their shortcomings. Section 3 discusses past research in related fields, demonstrates two previous attempts at improving texture alignment, and exhibits their inadequacies for our datasets. Section 4 presents our proposed seam minimization approach to texture mapping. Section 5 contains results and conclusions.

078
079

In all subsequent sections, we discuss the process of tex-

080
081

¹In this paper, we use the terms localization and pose recovery interchangeably, in that they both refer to recovering position and orientation.

082
083084
085086
087088
089090
091092
093094
095096
097098
099100
101102
103104
105106
107

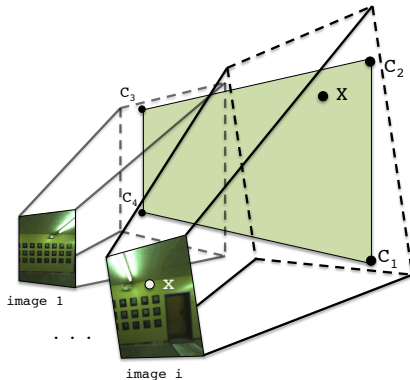


Figure 1: Planes are specified in 3D space by four corners C_1 to C_4 . Images are related to each plane through the camera matrices $P_{1..M}$.

ture mapping a single plane, as the texturing of each plane is independent and can be completed in parallel.

2. Tile-Based Texture Mapping

The geometry of the texture mapping process for a plane is shown in Figure 1. As described earlier, we are provided with a set of M images to texture the target plane. Each image has a camera matrix P_i for $i = 1..M$, which translates a 3D point in the world coordinate system to a 2D point or pixel in image i 's coordinates. A camera matrix P_i is composed of the camera's intrinsic parameters, such as focal length and image center, as well as extrinsic parameters which specify the rotation and translation of the camera's position in 3D world coordinates at the time that image i is taken. These extrinsic parameters are determined by the backpack hardware and localization algorithms [5, 16, 14] and are quite noisy.

Because the backpack system takes photos at a rate of 5 Hz, thousands of images are available for texturing each plane. Our goal in creating a texture mapping process is to decide which of these images should be used, and where their contents should map onto the texture, in order to eliminate any visual discontinuities or seams that would suggest that the plane's final texture is not composed of a single continuous image.

2.1. Direct Mapping

Ignoring the fact that the camera matrices $P_{1..M}$ are inaccurate, we can texture the plane by discretizing it into small square tiles, generally about 5 pixels across, and choosing an image to texture each tile.

We choose to work with rectangular units to ensure that borders between any two distinct images in the final texture are either horizontal or vertical. Since most environmental features inside buildings are horizontal or vertical, any

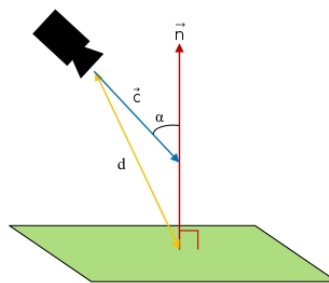


Figure 2: We minimize camera angle α and distance d by maximizing the scoring function $\frac{1}{d}(-1 \cdot \vec{c}) \cdot \vec{n}$

seams in our texture intersect them minimally and are likely to be less noticeable.

In order to select an image for texturing a tile t , we must first gather a list of candidate images that contain all four of its corners, which we can quickly check by projecting t into each image using the P_i camera matrices. Furthermore, each candidate image must have been taken at a time when its camera had a clear line-of-sight to t , which can be calculated using standard ray-polygon intersection tests between the camera location, the center of t , and every other plane [11].

Once we have a list of candidate images for t , we define a scoring function in order to objectively select the best image. Since camera pose errors compound over distance, we wish to minimize the distance between cameras and the plane they texture. Additionally, we desire images that are projected perpendicularly onto the plane, maximizing the resolution and amount of useful texture available in their projections, as well as minimizing any parallax effects. In other words, we wish to minimize the angle between the plane normal and the camera axis for images selected for texture mapping. These two criteria can be met by maximizing the function $\frac{1}{d}(-1 \cdot \vec{c}) \cdot \vec{n}$ as shown in Figure 2. Specifically, d is the distance between the centers of a camera and a tile, and \vec{n} and \vec{c} are the directions of the plane's normal and the camera axis respectively.

As Figure 3(a) demonstrates, this approach leads to the best texture for each tile independently, but overall results in many image boundaries with abrupt discontinuities, due to significant misalignment between images, as a result of camera pose inaccuracies.

2.2. Mapping with Caching

Since discontinuities occur where adjacent tiles select non-aligned images, it makes sense to take into account image selections made by neighboring tiles while texture mapping a given tile. By using the same image across tile boundaries, we can eliminate a discontinuity altogether. If this is not possible because a tile is not visible in images chosen by its neighbors, using similar images across tile

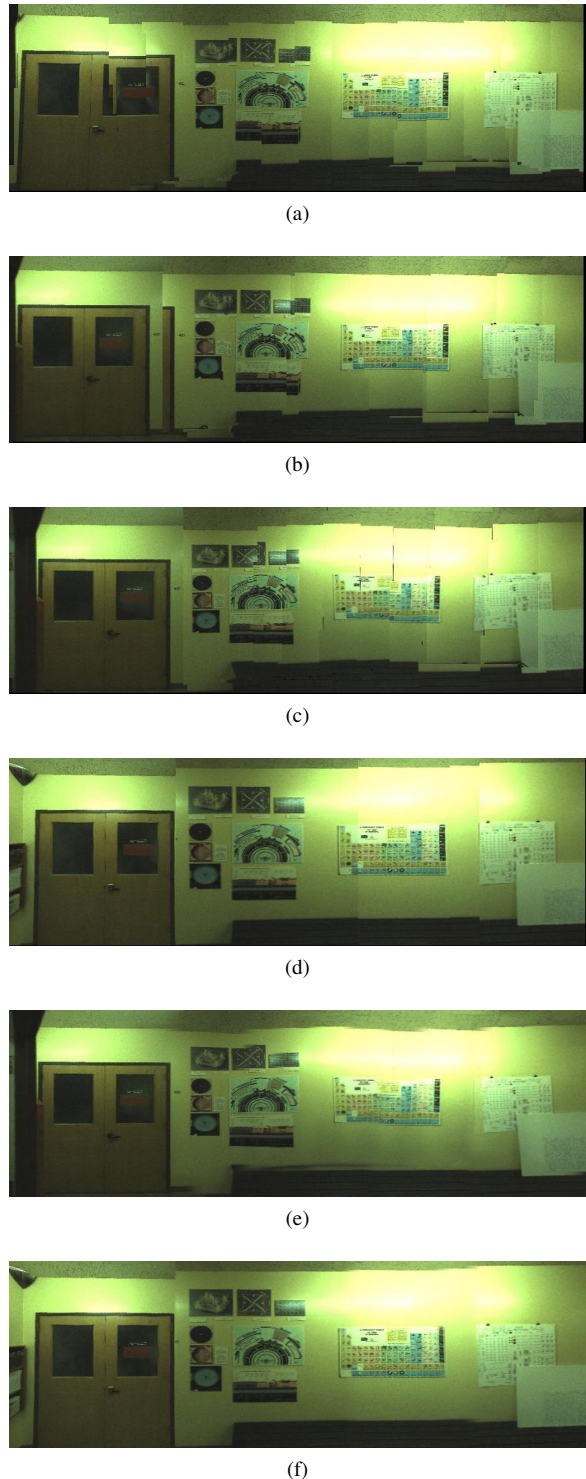


Figure 3: (a) Direct mapping. (b) Mapping with caching. (c) Mapping with caching after image alignment. (d) Seam minimization after image alignment. (e) same as (c) with blending. (f) same as (d) with blending.

boundaries also leads to less noticeable discontinuities.

Similar to a caching mechanism, we select the best image for a tile t by searching through two subsets of images for a viable candidate, before searching through the entire set. The first subset of images is those selected by adjacent tiles that have already been textured. We must first check which of these images can map to t , and then of those, we make a choice according to the scoring function in Figure 2. Before reusing this image, we ensure it meets the criteria $\alpha < 45^\circ$, in order to be considered a viable image, with α as the camera angle as shown in Figure 2.

If no satisfactory image is found in the first subset, we check the second subset of images, consisting of those taken near the ones in the first subset, both spatially and temporally. These images are not the same as the ones used for neighboring tiles, but are taken at a similar location and time, suggesting that their localization and projection are quite similar. Again, if no viable image is found according to the same criteria, we search the entire set of candidate images, selecting based on the same scoring function from Figure 2.

The result of this caching approach is shown in Figure 3(b). As compared to Figure 3(a), discontinuities are reduced overall, but the amount of remaining seams suggests that image selection alone cannot produce seamless textures. Camera matrices, or the image projections themselves have to be adjusted in order to reliably generate clean textures.

3. Existing Approaches to Image Alignment

In order to produce seamless texture mapping, either camera matrices need to be refined such that their localization is pixel accurate, or image stitching techniques need to be applied to provide this illusion.

Image projections can be aligned by refining their noisy camera poses, using image correspondences to adjust each image's camera matrix over 6 degrees of freedom (DOF) [7, 16, 21, 24]. Applying such approaches to our datasets however results in error accumulation and drift as shown in Figure 4(a), as well as high complexity and runtime [16].

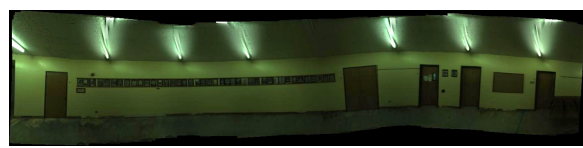
Another common approach to image alignment is to iteratively match images on intensity differences in selected patches, often in a spatial hierarchy [12, 18, 21, 23]. Another widely-used approach is to perform feature matching, which requires the detection of visual features and their existence in multiple images [4, 6, 19, 23, 26]. Notably, both approaches rely on the presence of multiple visual references, as when texturing detailed objects at high resolutions [2, 25], or when creating large scene panoramas [1, 2, 8, 22]. In contrast, our indoor datasets have a high prevalence of bare walls and ceilings, resulting in few reference points that can be used to judge alignment.

Additionally, our datasets often contain long chains of

216
217
218
219
220
221
222
223
224
225
226
227
228
229
230
231
232
233
234
235
236
237
238
239
240
241
242
243
244
245
246
247
248
249
250
251
252
253
254
255
256
257
258
259
260
261
262
263
264
265
266
267
268
269
270
271
272
273
274
275
276
277
278
279
280
281
282
283
284
285
286
287
288
289
290
291
292
293
294
295
296
297
298
299
300
301
302
303
304
305
306
307
308
309
310
311
312
313
314
315
316
317
318
319
320
321
322
323



(a)



(b)

Figure 4: Texture alignment via (a) the graph-based localization refinement algorithm from [5] and (b) image mosaicing.

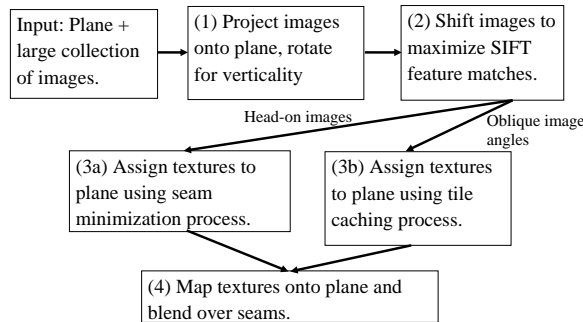


Figure 5: Our proposed method for seamless texture mapping.

images, which leads to error accumulation when image correspondences are not accurate. For example, when matching a long chain of images through homography, a pixel in the n th image must be translated into the first image's coordinates by multiplying by the 3×3 matrix $H_1H_2H_3\dots H_n$. Any error in one of these homography matrices is propagated to all further images, resulting in drift. Figure 4(b) shows the output of the AutoStitch software package, which performs homography-based image mosaicing [3]. Even with many features spread across this plane, the mosaicing produces errors that causes straight lines to appear as waves on the plane, despite the fact that it is generated after careful hand tuning. Many planes with fewer features simply failed outright using this approach.

4. Seamless Texture Mapping

In this section, we describe our proposed method for seamless texture mapping. Our approach consists of 4 steps, as seen in Figure 5. First, we project all images onto the plane and rotate them for verticality. Next, we perform

2D shifting in order to maximize SIFT feature matches in overlapping areas between these projections. We then select which textures to be used either with the tile caching method from Section 2.2, or with the more specialized method to be described in Section 4.3. This choice depends on the availability of head-on images for a given plane. We then finish by applying linear alpha blending to smooth out any remaining seams.

4.1. Image Rotation

We begin with the projection of all images onto the plane. This is done in the same way as in Section 2. Rather than work with all 6 DOF, which is computationally intensive, we choose to work only in two dimensions, performing 2D rotations and translations on the image projections, as errors in either lead to the greatest discontinuities.

We perform rotations using Hough transforms, which detect the presence and orientation of linear features in our images. Rather than match the orientation of such features in each image, we simply apply rotations such that the strongest near-vertical features are made completely vertical. This is effective for vertical planes in indoor models, since they usually consist of parallel vertical lines corresponding to doors, wall panels, rectangular frames, etc. If features in the area are not vertical, e.g. for floors and ceilings, this step is skipped.

4.2. Image Shifting

Our next step is to align overlapping images by searching for corresponding points between all pairs of overlapping images. We use SIFT features for their high detection rate, and choose to use feature alignment rather than intensity-based alignment due to the differences in lighting as well as possible occlusion among our images, both of which feature alignment is less sensitive to [15, 17, 19, 23].

SIFT matches determine d^x and d^y distances between each pair of features for two images on the plane, though these distances may not always be the same for different features. Since indoor environments often contain repetitive features such as floor tiles or doors, we need to ensure that SIFT-based distances are reliable. In order to mitigate the effect of incorrect matches and outliers, the RANSAC framework [10] is used for a robust estimate of the optimal $d_{i,j}^x$ and $d_{i,j}^y$ distances between two images i and j . The RANSAC framework handles the consensus-building machinery, and requires a fitting function and a distance function. For this application, the fitting function simply finds the average distance between matches in a pair of images. The distance function for a pair of points is chosen to be the difference between those points' SIFT match distance and the average distance computed by the fitting function. We use a 10 pixel outlier threshold, so that SIFT matches are labeled as outliers if their horizontal or vertical distances are

378
379
380
381
382
383
384
385
386
387
388
389
390
391
392
393
394
395
396
397
398
399
400
401
402
403
404
405
406
407
408
409
410
411
412
413
414
415
416
417
418
419
420
421
422
423
424
425
426
427
428
429
430
431

432 not within 10 pixels of the average distance computed by
 433 the fitting function.

434 We now use the $d_{i,j}^x$ and $d_{i,j}^y$ distances between each
 435 pair of images to refine their positions using least squares.
 436 Recall that there are a total of M^2 possible pairs of images,
 437 though we only generate distances between images
 438 that overlap at SIFT feature points. Given these distances
 439 and the original image location estimates, we can solve a
 440 least squares problem ($\min_{\vec{\beta}} \|A\vec{\beta} - \vec{\gamma}\|_2^2$) to estimate the
 441 location of the images on the plane. The M -dimensional vector
 442 $\vec{\beta}$ represents the unknown x location of each image on
 443 the plane for $1 \dots M$. The optimal x and y locations are ob-
 444 tained in the same way, so we only consider the x locations
 445 here:

$$\vec{\beta} = (x_1, x_2, x_3, \dots, x_{M-1}, x_M)$$

450 The $N \times (M + 1)$ dimensional matrix A is constructed
 451 with one row for each pair of images with measured
 452 distances produced by the SIFT matching stage. A row in the
 453 matrix has a -1 and 1 in the columns corresponding to the
 454 two images in the pair. For example, the matrix below indicates
 455 a SIFT-based distance between images 1 and 2, images
 456 1 and 3, images 2 and 3, etc.

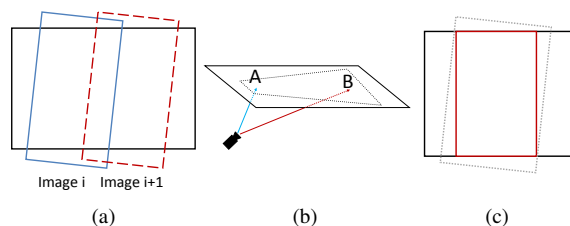
$$A = \begin{pmatrix} -1 & 1 & 0 & \dots & 0 & 0 \\ -1 & 0 & 1 & \dots & 0 & 0 \\ 0 & -1 & 1 & \dots & 0 & 0 \\ \vdots & \vdots & \vdots & \ddots & \vdots & \vdots \\ 0 & 0 & 0 & \dots & 1 & 0 \\ 0 & 0 & 0 & \dots & -1 & 1 \\ 1 & 0 & 0 & \dots & 0 & 0 \end{pmatrix}$$

466 If only relative distances between images are included then
 467 there is no way to determine the absolute location of any
 468 of the images and the matrix becomes rank deficient. To
 469 fix this we choose the first image to serve as the anchor for
 470 the rest, meaning all the absolute distances are based on its
 471 original location. This is done by adding a row with a 1 in
 472 the first column and the rest zeros.

473 Finally, the N -dimensional observation vector $\vec{\gamma}$ is con-
 474 structed using the SIFT-based distances generated earlier in
 475 the RANSAC matching stage. The last element in the ob-
 476 servation vector is the location of the first image determined
 477 by its original noisy localization, from [5, 16]. Thus $\vec{\gamma}$ can
 478 be written as:

$$\vec{\gamma}^T = (d_{1,2}, d_{1,3}, d_{2,3}, \dots, d_{N-2,N-1}, d_{N-1,N}, x_1)$$

483 The $\vec{\beta}$ that minimizes $\|A\vec{\beta} - \vec{\gamma}\|_2^2$ results in a set of image
 484 locations on the plane that best honors all the SIFT-based
 485 distance measurements between images. In practice there



486
 487
 488
 489
 490
 491
 492
 493
 494
 495
 496
 497
 498
 499
 500
 501
 502
 503
 504
 505
 506
 507
 508
 509
 510
 511
 512
 513
 514
 515
 516
 517
 518
 519
 520
 521
 522
 523
 524
 525
 526
 527
 528
 529
 530
 531
 532
 533
 534
 535
 536
 537
 538
 539

Figure 6: (a) Undistorted fisheye images for vertical planes are tilted, but their effective camera axis is more or less normal to the plane. (b) The effective camera axis for ceilings is at an angle with respect to the plane normal. (c) Wall images are cropped to be rectangular.

is often a break in the chain of images, meaning that no SIFT matches are found between one segment of the plane and another. In this case we add rows to the A matrix and observations to the $\vec{\gamma}$ vector that contain the original noisy x and y distance estimates from the original camera poses. Another way to do this is to add rows for all neighboring pairs of images and solve a weighted least squares problem where the SIFT distances are given a higher weight i.e. 1, and the noisy distances generated by the original camera poses [5, 16] are given a smaller weight e.g. 0.01.

After completing this same process for the y dimension as well, and making the resultant shifts, our images overlap and match each other with far greater accuracy. Applying the tile caching method from Section 2.2 on these rotated and shifted images results in the significant improvements shown in Figure 3(c), as compared to Figure 3(b).

4.3. Seam Minimization

As mentioned earlier, the mobile backpack system used to capture data in this paper contains 2 cameras with 180° fisheye lenses facing to the right and left. Since most human operators do not carry the backpack in a perfectly upright position and are bent forwards at 15 to 20 degrees with respect to the vertical direction, the undistorted fisheye images are head on with respect to vertical walls, but at an angle with respect to horizontal floors and ceilings. This is depicted for wall and ceiling planes in Figures 6(a) and 6(b) respectively. These oblique camera angles for ceilings translate into textures that span extremely large areas once projected, as shown in Figure 6(b). Using the tile-based texture mapping criteria from Figure 2, such projections have highly varying scores depending on the location on the plane, as shown in Figure 6(b). Thus, the tiling approach in Section 2 is a reasonable choice for texturing floors and ceilings, as it uses the parts of image projections that are viable choices for their respective plane locations, e.g. areas near point A in Figure 6(b), but not near point B.

For wall planes however, most images are taken from

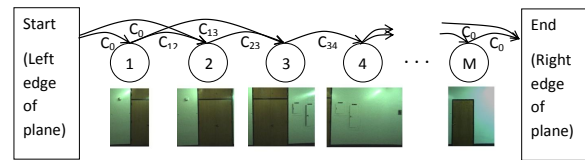
540 close distances and more or less head-on angles, resulting in
 541 higher resolution fronto-parallel projections. As a result, for
 542 each tile on a wall plane, the scoring function of Figure 2 is
 543 relatively flat with respect to a large number of captured im-
 544 ages, as they are all more or less head on. Thus, the scoring
 545 function is less significant for walls, and it is conceivable to
 546 use a different texturing strategy for them so as to minimize
 547 visible seams in texture mapped planes. This can be done
 548 by choosing the smallest possible set of images that (a) cov-
 549 ers the entire plane and (b) minimizes the amount of visible
 550 seams between them. A straightforward cost function that
 551 accomplishes the latter is the Sum of Squared Differences
 552 (SSD) of pixels in overlapping regions between all pairs of
 553 images, after they have been rotated as described in Sec-
 554 tion 4.1. Minimizing this cost function encourages image
 555 boundaries to occur either in featureless areas, such as bare
 556 walls, or in areas where images match extremely well.
 557

558 To cover the entirety of a plane, our problem can be de-
 559 fined as minimally covering a polygon i.e. the plane, using
 560 other polygons of arbitrary geometry i.e. image projections,
 561 with the added constraint of minimizing the cost function
 562 between chosen images. This is a complex problem, though
 563 we can take a number of steps to simplify it.

564 Given that wall-texture candidate images are taken from
 565 more or less head-on angles, and assuming only minor rota-
 566 tions are made in Section 4.1, we can reason that their pro-
 567 jections onto the plane are approximately rectangular. By
 568 cropping them all to be rectangular, as shown in Figure 6(c),
 569 our problem becomes the conceptually simpler one of fill-
 570 ing a polygon with rectangles, such that the sum of all costs
 571 between each pair of rectangles is minimal. We thus also
 572 retain the advantages of working with rectangular units, as
 573 explained in Section 2.

574 The location and orientation of the cameras and the fish-
 575 eye lenses on the acquisition backpack is such that images
 576 nearly always contain the entirety of the floor to ceiling
 577 range of wall planes. Images are therefore rarely projected
 578 with one above another when texturing wall planes. In
 579 essence, we need only to ensure lateral coverage of wall
 580 planes, e.g. from left to right, as our images provide full
 581 vertical coverage themselves. We can thus construct a Di-
 582 rected Acyclic Graph (DAG) from the images, with edge
 583 costs defined by the SSD cost function, and solve a simple
 584 shortest path problem to find an optimal subset of images
 585 with regard to the cost function [9].

586 Figure 7 demonstrates the construction of a DAG from
 587 overlapping images of a long hallway. Images are sorted
 588 by horizontal location left to right, and become nodes in
 589 a graph. Directed edges are placed in the graph from left
 590 to right between overlapping images. The weights of these
 591 edges are determined by the SSD cost function. Next, we
 592 add two artificial nodes, one start node representing the left
 593 border of the plane, and one end node representing the right



594
 595
 596
 597
 598
 599
 600
 601
 602
 603
 604
 605
 606
 607
 608
 609
 610
 611
 612
 613
 614
 615
 616
 617
 618
 619
 620
 621
 622
 623
 624
 625
 626
 627
 628
 629
 630
 631
 632
 633
 634
 635
 636
 637
 638
 639
 640
 641
 642
 643
 644
 645
 646
 647

Figure 7: DAG construction for the image selection process.

border of the plane. The left(right) artificial node has di-
 rected edges with equal cost C_0 to(from) all images that
 meet the left(right) border of the plane.

We now solve the shortest path problem from the start
 node to the end node. This results in a set of images com-
 pletely covering the plane horizontally, while minimizing
 the cost of seams between images.

In rare cases where the vertical dimension of the plane is
 not entirely covered by one or more chosen images, we are
 left with holes where no images are selected to texture. To
 address this, we solve for a new shortest path after modify-
 ing the edges chosen by the original shortest path solution
 such that they have higher cost than all other edges in the
 DAG, and solve for a new shortest path. This ensures that
 these edges are not chosen again unless they are the only
 available option. Our second shortest path solution results
 in a new set of chosen images, of which we only retain those
 that cover areas not covered by the first set. This process
 can be repeated as many times as needed, until holes are
 no longer present. This method is not as optimal as a 2D-
 coverage solution would be, but it is a fast approximation,
 and adequately handles the few holes we encounter.

With this completed, we have now mapped every loca-
 tion on the plane to at least one image, and have minimized
 the number of images, as well as the discontinuities between
 their borders. As seen in Figure 3(d), this seam minimiza-
 tion method has fewer visible discontinuities than Figure
 3(c) corresponding to the tile caching approach². This is es-
 pecially evident when comparing the posters in the images,
 which have clear misalignment over seams in Figure 3(c),
 but are much more aligned in Figure 3(d). This is because
 the seam minimization approach directly reduces the cost
 of each image boundary, while the tile caching method uses
 a scoring function that only approximates this effect. Fur-
 thermore, seam minimization guarantees the best selection
 of images, while the sequential tile caching method may se-
 lect images early on that turn out to be poor choices once
 subsequent tiles have been processed. The seam minimiza-
 tion approach is also far less intensive in terms of memory
 usage and runtime, both during texture generation and ren-

²In Figure 3(d), we arbitrarily chose one image for texturing where images overlap, as blending will be discussed in the next section.

648 dering, as it does not require discretizing planes or images³.
 649 In the context of texturing an entire 3D planar model, we
 650 choose to apply the seam minimization approach on walls,
 651 due to its superior output when provided with head-on im-
 652 ages. Floors and ceilings however, given their many images
 653 taken at oblique angles, are textured using the tile caching
 654 method.
 655

4.4. Blending

We now apply the same blending process to the two tex-
 657 turing methods: image alignment followed by either tile
 658 caching or seam minimization.
 659

Although the preprocessing steps and image selection in
 660 both methods attempt to minimize all mismatches between
 661 images, there are occasional unavoidable discontinuities in
 662 the final texture due to different lighting conditions or inac-
 663 curacies in planar geometry or projection. These can how-
 664 ever be treated and smoothed over by applying alpha blend-
 665 ing over image seams. Whether the units we are blending
 666 are rectangularly-cropped images or rectangular tiles, we
 667 can apply the same blending procedure, as long as we have
 668 a guaranteed overlap between units to blend over.
 669

For the tile caching method, we can ensure overlap by
 670 texturing a larger tile than needed for display. For example,
 671 for a rendered tile $l_1 \times l_1$, we can associate it with a texture
 672 $(l_1 + l_2) \times (l_1 + l_2)$ in size. For the seam minimization
 673 method, we have already ensured overlap between images.
 674 To enforce consistent blending however, we add a mini-
 675 mum required overlap distance while solving the shortest
 676 path problem in Section 4.3. Additionally, if images over-
 677 lap in a region greater than the overlap distance, we only
 678 apply blending over an area equal to the overlap distance.
 679

After blending pixels linearly across overlapping regions
 680 using alpha blending, texture mapping is complete. Figures
 681 3(e) and 3(f) show the blended versions of Figures 3(c) and
 682 3(d) respectively. It is clear that the seam minimization
 683 approach still exhibits better alignment and fewer seams than
 684 the tile-caching method, as Figure 3(f) has the best visual
 685 quality among the textures in Figure 3.
 686

5. Results and Conclusions

Examples of ceilings and floors textured with the tile
 690 caching approach, and walls textured with the seam mini-
 691 mization approach, are displayed in Figure 8. High reso-
 692 lution texture comparisons, as well as a walkthrough of a
 693 fully textured 3D model are available in the accompanying
 694 video to this paper.
 695

³For the seam minimization approach, occlusion checks are performed
 696 over the entirety of each image to determine available areas for texture
 697 mapping. Since indoor environments mostly consist of vertical or horizontal
 698 surfaces with high amounts of right angles, image projections remain
 699 largely rectangular after masking out occluded areas. Therefore, as a pre-
 700 processing step, we can recursively split each image into rectangular pieces
 701 and check for occlusions in a similar manner as in the tiling process.

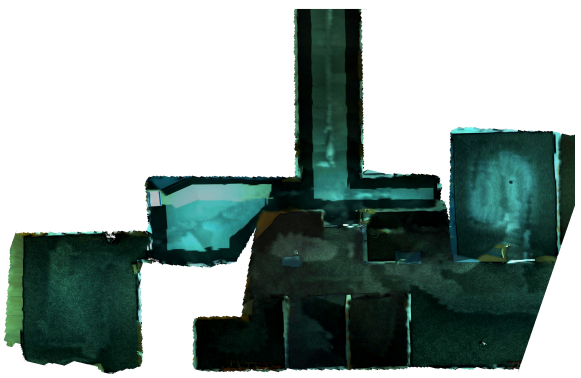
In this paper, we have developed an approach to texture
 702 map models with noisy camera localization data. We are
 703 able to refine image locations based on feature matching,
 704 and robustly handle outliers. The tile-based mapping ap-
 705 proach can be used to texture both simple rectangular walls
 706 as well as complex floor and ceiling geometry. We also pre-
 707 sented a seam minimization texturing method that produces
 708 seamless textures on planes where multiple head-on images
 709 are available. Each of these approaches is highly modular,
 710 and easily tunable for different environments and acquisi-
 711 tion hardware.
 712

References

- [1] A. Agarwala, M. Agrawala, M. Cohen, D. Salesin, and R. Szeliski. Photographing long scenes with multi-viewpoint panoramas. In *ACM Transactions on Graphics (TOG)*, volume 25, pages 853–861. ACM, 2006. 3
- [2] F. Bernardini, I. Martin, and H. Rushmeier. High-quality texture reconstruction from multiple scans. *Visualization and Computer Graphics, IEEE Transactions on*, 7(4):318–332, 2001. 3
- [3] M. Brown and D. Lowe. Autostitch. <http://www.cs.bath.ac.uk/brown/autostitch/autostitch.html>. 4
- [4] M. Brown and D. Lowe. Automatic panoramic image stitching using invariant features. *International Journal of Computer Vision*, 74(1):59–73, 2007. 3
- [5] G. Chen, J. Kua, S. Shum, N. Naikal, M. Carlberg, and A. Zakhor. Indoor localization algorithms for a human-operated backpack system. In *Int. Symp. on 3D Data, Processing, Visualization and Transmission (3DPVT)*. Citeseer, 2010. 1, 2, 4, 5
- [6] S. Cho, Y. Chung, and J. Lee. Automatic image mosaic system using image feature detection and taylor series. In *Proceedings of the 7th International Conference on Digital Image Computing: Techniques and Applications*, pages 549–556, 2003. 3
- [7] S. Coorg and S. Teller. Matching and pose refinement with camera pose estimates. In *Proceedings of the 1997 Image Understanding Workshop*, 1997. 3
- [8] P. Debevec, Y. Yu, and G. Borshukov. Efficient view-dependent image-based rendering with projective texture-mapping. In *Eurographics Rendering Workshop*, volume 98, pages 105–116, 1998. 3
- [9] E. Dijkstra. A note on two problems in connexion graphs. *Numerische Mathematik*, 1:269–271, 1959. 6
- [10] M. Fischler and R. Bolles. Random sample consensus: a paradigm for model fitting with applications to image analysis and automated cartography. *Communications of the ACM*, 24(6):381–395, 1981. 4
- [11] A. Glassner et al. *An introduction to ray tracing*. Academic Press, 1989. 2
- [12] G. Hager and P. Belhumeur. Efficient region tracking with parametric models of geometry and illumination. *Pattern Analysis and Machine Intelligence, IEEE Transactions on*, 20:1025–1039, 1998. 3



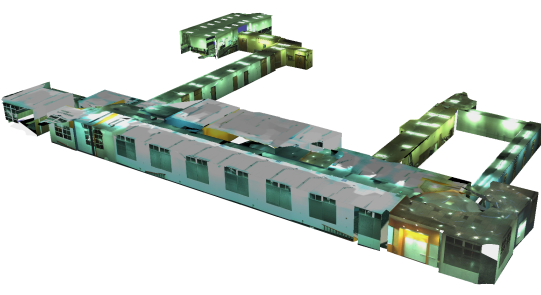
(a)



(c)



(b)



(d)

Figure 8: Examples of our final texture mapping output for (a) walls, (b) ceilings, (c) an entire floor, (d) a full model.

- [784] R. Hartley and A. Zisserman. *Multiple view geometry in computer vision*, volume 2. Cambridge Univ Press, 2000. 1
- [785] J. Kua, N. Corso, and A. Zakhor. Automatic loop closure detection using multiple cameras for 3d indoor localization. In *IS&T/SPIE Electronic Imaging*, 2012. 1, 2
- [786] S. Lai and M. Fang. Robust and efficient image alignment with spatially varying illumination models. In *Computer Vision and Pattern Recognition, 1999. IEEE Computer Society Conference on.*, volume 2. IEEE, 1999. 4
- [787] T. Liu, M. Carlberg, G. Chen, J. Chen, J. Kua, and A. Zakhor. Indoor localization and visualization using a human-operated backpack system. In *Indoor Positioning and Indoor Navigation (IPIN), 2010 International Conference on*, pages 1–10. IEEE, 2010. 1, 2, 3, 5
- [788] D. Lowe. Object recognition from local scale-invariant features. In *Computer Vision, 1999. The Proceedings of the Seventh IEEE International Conference on*, volume 2, pages 1150–1157. Ieee, 1999. 4
- [789] B. Lucas and T. Kanade. An iterative image registration technique with an application to stereo vision. In *Proceedings of the 7th international joint conference on Artificial intelligence*, 1981. 3
- [790] K. Mikolajczyk and C. Schmid. A performance evaluation of local descriptors. *Pattern Analysis and Machine Intelligence, IEEE Transactions on*, 27(10):1615–1630, 2005. 3, 4

- [791] V. Sanchez and A. Zakhor. Planar 3d modeling of building interiors from point cloud data. In *International Conference on Image Processing*, 2012. 1
- [792] H. Shum and R. Szeliski. Systems and experiment paper: Construction of panoramic image mosaics with global and local alignment. *International Journal of Computer Vision*, 36:101–130, 2000. 3
- [793] N. Snavely, S. Seitz, and R. Szeliski. Photo tourism: exploring photo collections in 3d. In *ACM Transactions on Graphics (TOG)*, volume 25, pages 835–846. ACM, 2006. 3
- [794] R. Szeliski. Image alignment and stitching: A tutorial. *Foundations and Trends® in Computer Graphics and Vision*, 2(1):1–104, 2006. 3, 4
- [795] R. Szeliski and H. Shum. Creating full view panoramic image mosaics and texture-mapped models. In *SIGGRAPH 95*, pages 251–258. ACM SIGGRAPH, 1997. 3
- [796] L. Wang, S. Kang, R. Szeliski, and H. Shum. Optimal texture map reconstruction from multiple views. In *Computer Vision and Pattern Recognition, 2001. CVPR 2001. Proceedings of the 2001 IEEE Computer Society Conference on*, volume 1, pages I–347. IEEE, 2001. 3
- [797] G. Yun Tian, D. Gledhill, and D. Taylor. Comprehensive interest points based imaging mosaic. *Pattern recognition letters*, 24:1171–1179, 2003. 3